

Differences in the acoustic characteristics of DC bias alternating arcs in argon, helium, and nitrogen

Yutai Li(李雨泰), Qinghao Wen(文清皓), Yangyang Fu(付洋洋), Xiaobing Zou(邹晓兵), Handong Li(黎晗东), Zhigang Liu(刘志刚), Haiyun Luo(罗海云), Dun Qian(钱盾), Zhe Chen(陈喆), and Xinxin Wang(王新新)

Citation: Chin. Phys. B, 2024, 33 (**12**): 125204. DOI: 10.1088/1674-1056/ad8070
Journal homepage: http://cpb.iphy.ac.cn; http://iopscience.iop.org/cpb

What follows is a list of articles you may be interested in

Ion acoustic solitary waves in an adiabatic dusty plasma: Roles of superthermal electrons, ion loss and ionization

Qianghua Rao(饶强华), Hui Chen(陈辉), Sanqiu Liu(刘三秋), and Xiaochang Chen(陈小昌)
Chin. Phys. B, 2024, 33 (**8**): 085201. DOI: 10.1088/1674-1056/ad47e4

Influence of low ambient pressure on the performance of a high-energy array surface arc plasma actuator

Bing-Liang Tang(唐冰亮), Shan-Guang Guo(郭善广), Hua Liang(梁华)†, and Meng-Xiao Tang(唐孟潇)
Chin. Phys. B, 2020, 29 (**10**): 105204. DOI: 10.1088/1674-1056/aba9c8

Experimental investigation on electrical characteristics and ignition performance of multichannel plasma igniter

Sheng-Fang Huang(黄胜方), Hui-Min Song(宋慧敏), Yun Wu(吴云), Min Jia(贾敏), Di Jin(金迪), Zhi-Bo Zhang(张志波), Bing-Xuan Lin(林冰轩)
Chin. Phys. B, 2018, 27 (**3**): 035203. DOI: 10.1088/1674-1056/27/3/035203

Growth of small diameter multi-walled carbon nanotubes by arc discharge process

K. T. Chaudhary, J. Ali, P. P. Yupapin
Chin. Phys. B, 2014, 23 (**3**): 035203. DOI: 10.1088/1674-1056/23/3/035203

Investigation on the shockwave induced by surface arc plasma in quiescent air

Jin Di (金迪), Li Ying-Hong (李应红), Jia Min (贾敏), Li Fan-Yu (李凡玉), Cui Wei (崔巍), Sun Quan (孙权), Zhang Bai-Ling (张百灵), Li Jun (李军)
Chin. Phys. B, 2014, 23 (**3**): 035201. DOI: 10.1088/1674-1056/23/3/035201

Differences in the acoustic characteristics of DC bias alternating arcs in argon, helium, and nitrogen

Yutai Li(李雨泰)[1,3,†], Qinghao Wen(文清皓)[1], Yangyang Fu(付洋洋)[3], Xiaobing Zou(邹晓兵)[3], Handong Li(黎晗东)[4], Zhigang Liu(刘志刚)[5], Haiyun Luo(罗海云)[3], Dun Qian(钱盾)[6], Zhe Chen(陈喆)[2,3,‡], and Xinxin Wang(王新新)[3]

[1] *Xuefeng Mountain Energy Equipment Safety National Observation and Research Station, Chongqing University, Chongqing* 400044, *China*
[2] *China Huaneng Group Co., Ltd., Beijing* 100031, *China*
[3] *Department of Electrical Engineering, Tsinghua University, Beijing* 100084, *China*
[4] *China Three Gorges Renewables (Group) Co., Ltd., Beijing* 101199, *China*
[5] *School of Electrical Engineering, Xi'an Jiaotong University, Xi'an* 710049, *China*
[6] *Electric Power Research Institute, State Grid Zhejiang Electric Power Co., Ltd., Hangzhou* 310014, *China*

(Received 19 July 2024; revised manuscript received 25 September 2024; accepted manuscript online 27 September 2024)

The acoustic effects of gas discharge plasma have received much attention. Previous studies have shown that cold plasma and thermal plasma have different principles of sound generation. In this paper, the differences in the acoustic characteristics of DC bias alternating arc plasma (thermal plasma) in different gas environments (argon, helium, and nitrogen) are investigated by combining experiments and simulations. Many processes in industrial machining involve this arc plasma. It was found that the acoustic characteristics of the arcs of these three gases are significantly different. The two key parameters, electrical and thermal conductivity of the gas, determine the acoustic characteristics of the arc by influencing the electric power of the arc and the heat dissipation through the anode. At the same drive current, the nitrogen arc has the largest voltage drop and the helium arc has the highest electroacoustic conversion efficiency. This results in the acoustic pressure amplitude being helium, nitrogen, and argon in descending order. The research contributes to a deeper understanding of the vocalization mechanism of arc plasma and provides theoretical guidance on gas selection for arc acoustic wave applications.

Keywords: arc discharge, gas discharge and plasma, arc acoustic wave, acoustic characteristics

PACS: 52.80.Mg, 52.80.Tn, 52.25.Kn, 52.77.Fv **DOI:** 10.1088/1674-1056/ad8070

1. Introduction

When the internal state of a gas discharge plasma changes (e.g., when the energy injected into the plasma changes due to fluctuations in the discharge current or voltage), it is often accompanied by the generation of sound waves.[1] The acoustic process of the discharge plasma can be analogized to that of a mechanical loudspeaker, as shown in Fig. 1. In the mechanical loudspeaker, the audio current through the coil generates an alternating magnetic field that vibrates the magnet, driving the diaphragm to push the air to vibrate. This gas pressure change propagates from the sound source in the form of sound. If the mechanical system is replaced by ionized gas, the plasma can be regarded as the sum of coil and magnet. When the current injected into the plasma changes, the energy or momentum of charged particles will be transferred to the surrounding air molecules, resulting in air vibration. This gas pressure change can also be propagated from the plasma in the form of sound waves.[2]

The acoustic phenomenon of gas discharge plasma was first found in radio frequency spark discharge,[3] and then people have successively detected acoustic wave generation in various discharge forms such as corona discharge, glow discharge, and arc discharge.[4–6] Discharge plasma acoustic waves have a wide range of applications, including plasma loudspeakers, pulsed sound sources, corona noise monitoring of transmission lines, plasma arc cutting status monitoring, arc welding and arc furnace combustion status monitoring, arc ultrasonic emission, substation and electric aircraft fault arc diagnosis.[7–11]

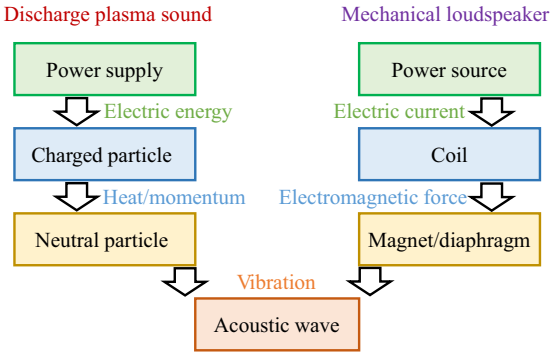


Fig. 1. Technical principle of discharge plasma sound and mechanical loudspeakers.

Discharge plasma can be divided into cold plasma and

†Corresponding author. E-mail: liyt@cqu.edu.cn
‡Corresponding author. E-mail: 287195465@qq.com

© 2024 Chinese Physical Society and IOP Publishing Ltd

thermal plasma.[12,13] The plasma with low ionization degree of gas is usually cold plasma, and its electron temperature is high (up to tens of thousands), while the temperature of heavy particles (ions and gas particles) is low and close to room temperature, that is, the components of the plasma are in a non-thermal equilibrium state.[14] On the contrary, plasma with high ionization degree of gas is usually thermal plasma, and its constituent particles have the same and higher temperature (thousands or even tens of thousands of degrees), that is, the constituent particles of plasma are in thermal equilibrium.[15] Whether it is a cold plasma or a thermal plasma, as long as the electric energy injected into the plasma changes, sound waves can be generated. However, the principle of sound waves generated by the two types of plasma is different, which is reflected in the fact that the energy or momentum of charged particles in the plasma is transferred to the surrounding air molecules differently. At present, it is believed that there are two sound generation mechanisms in the discharge plasma:

(i) The momentum transfer from charged particles to gas particles causes sound waves.[16] This momentum transfer mainly comes from the elastic collision between moving charged particles and gas particles, which is usually called "momentum modulation".

(ii) The energy transfer from charged particles to gas particles causes sound waves,[17] which are often referred to as "energy modulation".

In general, momentum modulation is dominant in cold plasma. In thermal plasma, only energy modulation is generally considered.

This study mainly focuses on arc plasma (thermal plasma) sound. The processes of welding, spraying, and smelting in the field of industrial processing involve time-varying arc plasma, which generates acoustic waves that can be hazardous to the hearing health of workers. In addition, its acoustic properties can also reflect the performance of the process to a certain extent. Therefore, the acoustic properties of time-varying arc plasma have been widely concerned. The current research on arc plasma acoustic wave has primarily emphasized its diverse applications,[18–20] but there is insufficient investigation into the inherent characteristics and physical processes of the arc acoustic wave itself.

Because different gases have different electrical and thermodynamic properties,[21] they may have different effects on the discharge plasma acoustic wave. In 1987, Mazzola *et al.* compared the acoustic frequency response of air, argon and helium when studying the acoustic wave of DC glow discharge, and found that the intensity of the acoustic wave generated by glow discharge was argon, air, and helium in order.[22] However, glow discharge produces cold plasma, while arc discharge produces thermal plasma. The mechanism of sound waves produced by the two kinds of plasma is different. Therefore, the influence of background gas on glow discharge sound wave may be different from that on arc sound wave. Up to now, there is no research report on the influence of background gas on arc sound wave.

In this paper, the acoustic characteristics of DC bias alternating arcs in argon, helium, and nitrogen, which are widely used in industry, are studied through experiments and numerical simulation, and the effects of gas conductivity and thermal conductivity on the sound characteristics are summarized, and the physical explanation is given.

2. Experimental setup

"Pure AC arc" means the arc in which the current waveform is symmetrical and oscillates periodically, with the current crossing the zero point once per half cycle.[1] If the above "pure AC arc" current superimposed on a DC component, so that the total current waveform does not pass through the zero point, it is called "DC bias alternating arc".[23] It can solve the problem of the arc "extinguished by zero point". Its advantage is that it is easy to stabilize the combustion, even with a small current of about 100 A, can maintain a long (10 mm or so) arc. Therefore, we chose the TIG welding machine WS-315 produced by Zhejiang Hufeng Brand to generate DC-biased alternating arc. The typical current waveform of the DC-biased rectangular wave alternating current output from this power supply is shown in Fig. 2. I_{DC} and I_{AC} are the DC and AC components of the current respectively. The adjustment range of DC component and AC component is 0–100 A and 0–80 A respectively, and the adjustment range of AC component frequency is 20 Hz–250 Hz. When adjusting the current, only need to control $I_{DC} > I_{AC}$, it can realize that the current is always greater than zero, avoiding arc quenching.

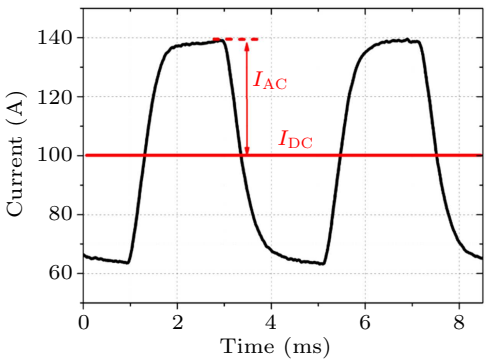


Fig. 2. Current waveform.

The equipment arrangement is shown in Fig. 3. The cathode is the tungsten needle of the welding torch, which emits gas to protect the cathode and stabilize the combustion. The anode is the grounding electrode. The anode is made of graphite for the following reasons: firstly, graphite is resistant to ablation, and secondly, graphite has a low hardness, so that if ablation occurs (e.g., after a prolonged discharge), the

abraded area can be removed by simple wiping. It is important to note that although graphite is relatively ablation-resistant, its structure undergoes some changes (from a circular cone to a circular truncated cone) after many discharges. This means that its top will become flat, so we use a tip-plate geometry in the subsequent simulation model.

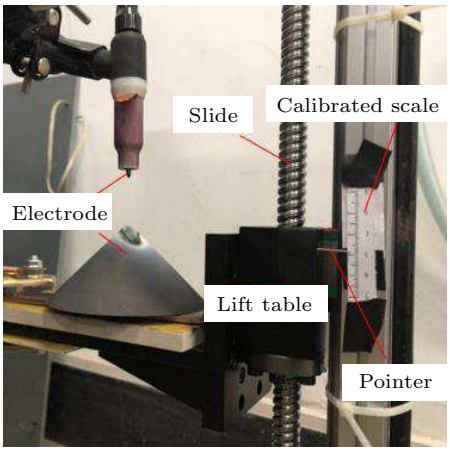


Fig. 3. Equipment arrangement.

Current waveforms are measured using the Lecroy CP150 current probe, which can measure a maximum continuous current of 150 A with a bandwidth of 10 MHz to meet the measurement requirements. The voltage waveforms are measured using the Lecroy PP009 voltage probe, which can measure a maximum voltage of 500 V with a bandwidth of 500 MHz. The acoustic waveforms are measured using an RST6000 microphone from RSTECH (BEIJING) Co., Ltd. The microphone is aligned to the center of the arc axis and arranged at 15 cm from the arc axis. The microphone bandwidth is 20 Hz to 16 kHz and the sensitivity is 33.15 Pa/mV.

3. Numerical model

Establishing and solving the numerical model is done in COMSOL Multiphysics. The default solver is used for the solution. The criterion for convergence is that the variables reach stability. Mesh-independence tests are also performed to ensure the reliability of the results.

3.1. Arc plasma model

Arc plasma is essentially a magnetic fluid and can be described mathematically using hydrodynamics and electromagnetism. The mathematical equations for arc plasma are generally based on the following assumptions given below.

(i) The arc plasma is in local thermodynamic equilibrium (LTE).[24] The electromagnetic and thermodynamic parameters of the arc are considered to be functions of temperature and pressure.

It should be noted that practically full thermodynamic equilibrium can only be reached in a blackbody cavity. In an arc plasma, important parameters include temperature and particle density. As long as their gradients are satisfied to be small, the arc plasma can be considered to be in LTE.[25]

(ii) The arc is two-dimensional (2D) axisymmetric and can be solved by establishing a 2D axisymmetric model in a cylindrical coordinate system.[26] This is due to the fact that the electrode structure used is axisymmetric, and then the arc should also be axisymmetric without considering other factors.

(iii) The arc is optically thin. This is because the reabsorption of radiation is insignificant compared to the total radiation loss at all wavelengths.[27]

(iv) The arc is in a stable combustion state without considering the process of arc initiation.[1] This is due to the fact that only stable combustion state is studied in this paper.

(v) The arc is in a laminar flow state with no turbulence.[24] The reason for this is that the flow state of an arc in a stable combustion state is relatively steady.

(vi) The effect of gravity and heat dissipation due to viscosity in the arc are small and negligible.

Based on the above assumptions, the equations to be solved are as follows:

(I) Current continuity equation

$$\frac{\partial j_z}{\partial z}+\frac{1}{r}\frac{\partial (rj_r)}{\partial r}=0, \tag{1}$$

where j_r and j_z are the radial and axial current densities, respectively.

(II) Ohm's law

$$j_z=\sigma\frac{\partial \varphi}{\partial z},\quad j_r=\sigma\frac{\partial \varphi}{\partial r}, \tag{2}$$

where σ and φ are conductivity and potential, respectively.

(III) Ampere circuital theorem

$$B_\theta=\frac{\mu}{r}\int_0^r j_z\xi\,\mathrm{d}\xi, \tag{3}$$

where μ and B_θ are the magnetic permeability and magnetic induction, respectively.

(IV) Mass conservation equation

$$\frac{\partial \rho}{\partial t}+\frac{\partial(\rho u)}{\partial z}+\frac{1}{r}\frac{\partial(\rho r v)}{\partial r}=0, \tag{4}$$

where u, v, and ρ are the axial and radial velocity components and mass density, respectively.

(V) Momentum conservation equation

$$\begin{aligned}&\rho\frac{\partial u}{\partial t}+\rho u\frac{\partial u}{\partial z}+\rho v\frac{\partial u}{\partial r}\\&=-\frac{\partial p}{\partial z}+2\frac{\partial}{\partial z}\left(\eta\frac{\partial u}{\partial z}\right)+\frac{1}{r}\frac{\partial}{\partial r}\left(\eta r\frac{\partial u}{\partial r}\right)\\&\quad+\frac{1}{r}\frac{\partial}{\partial r}\left(\eta r\frac{\partial v}{\partial z}\right)+j_r\times B_\theta,\\&\rho\frac{\partial v}{\partial t}+\rho u\frac{\partial v}{\partial z}+\rho v\frac{\partial v}{\partial r}\\&=-\frac{\partial p}{\partial r}+\frac{\partial}{\partial z}\left(\eta\frac{\partial v}{\partial z}\right)+\frac{2}{r}\frac{\partial}{\partial r}\left(\eta r\frac{\partial v}{\partial r}\right)\end{aligned}$$

$$+\frac{\partial}{\partial z}\left(\eta\frac{\partial u}{\partial r}\right)-\frac{2\eta v}{r^2}-j_z\times B_\theta, \tag{5}$$

where p and η are the pressure and viscosity, respectively.

(VI) Energy conservation equation

$$\begin{aligned}&\rho C_{\rm V}\frac{\partial T}{\partial t}+\rho C_{\rm V}u\frac{\partial T}{\partial z}+\rho C_{\rm V}v\frac{\partial T}{\partial r}\\&=\lambda\frac{\partial^2 T}{\partial z^2}+\lambda\frac{1}{r}\frac{\partial}{\partial r}\left(r\frac{\partial T}{\partial r}\right)+\frac{j_z^2+j_r^2}{\sigma}\\&+\frac{5}{2}\frac{k_{\rm b}}{e}\left(j_z\frac{\partial T}{\partial z}+j_r\frac{\partial T}{\partial r}\right)-S_{\rm R},\end{aligned} \tag{6}$$

where $C_{\rm V}$, T, λ, $S_{\rm R}$, $k_{\rm b}$ are the heat capacity at constant volume, the temperature, the thermal conductivity, the thermal radiation term, and the Boltzmann constant, respectively.

The mass density can be expressed by the ideal gas state equation as follows:

$$\rho=\frac{pM}{RT}, \tag{7}$$

where M is the molar mass of air and R is the gas constant.

The thermal radiation term of the arc can be expressed as follows:

$$S_{\rm R}=4\alpha k\left(T^4-T_0^4\right), \tag{8}$$

where $k=13\,(p/p_0)\ {\rm m}^{-1}$ ($p_0=1$ atm, 1 atm = 1.01325×10^5 Pa) is the absorption coefficient, α is the Stefan–Boltzmann constant with a value of 5.67×10^{-8} W/(m^2·K^4), and T_0 is the ambient temperature with a value of 300 K.

In the numerical simulation of arc plasma in this paper, the field-circuit coupling calculation method is used. The arc and electrode parts are modelled by magnetohydrodynamics, and the electrode boundary is connected to the external circuit as a port (U–I port).

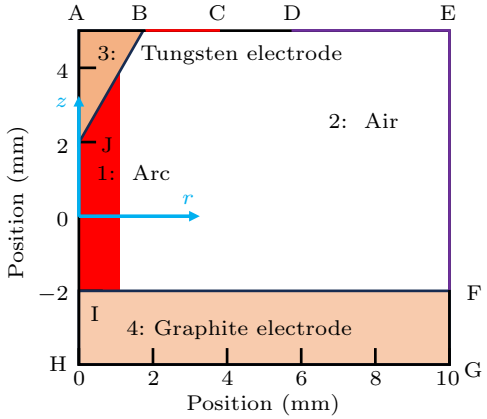


Fig. 4. The arc and electrode calculation domain.

The arc and electrode calculation domain selected in this paper is shown in Fig. 4. For the convenience of describing the spatial location, r is defined as the radial coordinate, z is the axial coordinate, and the coordinate origin is located at the center of the arc. The regions 1 and 2 are the initially set arc region and air region, respectively. The arc length is 4 mm. region 3 is the tungsten electrode part (cathode) and region 4 is the graphite electrode part (anode). The axial coordinates of the anode surface I–F are $z=-2$, and the axial coordinates of the cathode tip J are $z=2$. A–B and H–G are connected as ports to the external circuit. B–C is the protective gas inflow interface (length 2 mm), C–D is the nozzle wall (length 2 mm), and D–E–F is the air interface.

A non-uniform grid is used for the computational domain. Since region 1 is an arc region with large temperature and current density variations along the axial and radial directions, a higher mesh density is used to obtain an accurate numerical solution. Whereas in other regions where physical quantities vary less, lower grid densities are used. A reasonable balance between the accuracy and the amount of calculation is achieved.

The external circuit is shown in Fig. 5 and includes the power supply, resistance, and inductance. The same arc current waveform as the experiment can be obtained by adjusting the circuit parameters.

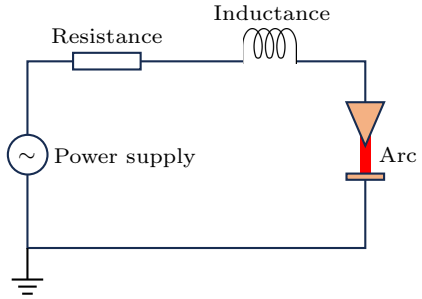


Fig. 5. The external circuit.

The various boundary conditions in the numerical calculations are shown in Table 1. Although there may be slight differences between the defined boundary temperature values and the actual boundary temperature values, they are relatively small compared to the high temperatures of tens of thousands of Kelvins at the center of the arc. Therefore, the temperature error on the boundary will not have a significant effect on the arc temperature characteristics. The rate of the protective airflow was set to 40 L/min in the experiment.

After defining the boundary conditions, the initial values of the physical quantities need to be given. Among them, potential, velocity, and pressure can be set to zero. The setting of the temperature physical quantity is more complicated. In the air region, the initial temperature can be set to 300 K. The initial value for the temperature in the arc region is set to 10^4 K. This is because the conductivity of the arc starts to increase significantly above 5000 K. If the initial value is set too low, the arc channel will not be able to conduct electricity at the beginning. The initial temperature in the electrode region is set to 2000 K. The actual temperature distribution in these regions will be obtained through simulation.

Table 1. Boundary conditions.

	AH	AB	BC	CD	DE	EF	FGH	IF	BJ
φ (V)	$\frac{\partial\varphi}{\partial r}=0$	circuit	$\frac{\partial\varphi}{\partial z}=0$	$\frac{\partial\varphi}{\partial z}=0$	$\frac{\partial\varphi}{\partial z}=0$	$\frac{\partial\varphi}{\partial r}=0$	circuit	–	–
u (m/s)	$\frac{\partial u}{\partial r}=0$	–	u_{gas}	0	–	–	–	0	0
v (m/s)	0	–	0	0	–	–	–	0	0
p (atm)	–	–	–	–	1	1	–	–	–
T (K)	$\frac{\partial T}{\partial r}=0$	5000 K	1000 K	1000 K	1000 K	1000 K	2000 K	–	–

3.2. Acoustic model

Due to the small amplitude of the arc acoustic wave (generally less than 140 dB), the sound field can be mathematically described by the small amplitude acoustic wave equation, which is generally based on the following assumptions:

(i) The medium is an ideal fluid without viscosity.

(ii) During the propagation of sound waves, the continuous compression and expansion of the medium causes temperature fluctuations, resulting in differences in temperature at different spatial locations. Since the vibration frequency of the medium is relatively high during the propagation of sound waves, it is too late for heat exchange to take place between different regions. In other words, the propagation of sound waves is adiabatic (isentropic process).

(iii) The amplitude of sound waves is so small that the propagation of sound waves can be analyzed using linear acoustic methods.

Based on the above assumptions, the equations to be solved are as follows:

(I) Continuity equation

$$\frac{\partial\rho'}{\partial t}+\rho_0\left(\frac{\partial u}{\partial z}+r\frac{\partial v}{\partial r}\right)=0, \tag{9}$$

where ρ' is the mass density perturbation, equal to ρ–ρ_0, and ρ_0 is the static mass density in the absence of perturbation.

(II) Motion equations

$$\rho_0\frac{\partial u}{\partial t}+\frac{\partial p'}{\partial z}=0,\quad \rho_0\frac{\partial v}{\partial t}+\frac{\partial p'}{\partial r}=0, \tag{10}$$

where p' is the pressure perturbation, equal to p–p_0, and p_0 is the ambient air pressure. According to the definition of sound pressure, p' is the sound pressure.

The general form of the acoustic wave equation can be obtained from Eqs. (9) and (10):

$$\frac{\partial^2\rho'}{\partial t^2}=\nabla^2 p'. \tag{11}$$

(III) Equation of state

In the region outside the source, sound waves are considered adiabatic processes (isentropic processes). The density is then only a function of the pressure

$$\rho=f(p). \tag{12}$$

However, the arc region does not fulfil the adiabatic (isentropic) condition. Its density is not only a function of pressure, but also of entropy s (entropy change is generated by the heat fed into it):

$$\rho=f(p,s). \tag{13}$$

According to the full differential equation and the small perturbation condition, equation (13) can be derived as

$$\begin{aligned}
&\rho'=\left(\frac{\partial\rho}{\partial p}\right)_s p'+(\frac{\partial\rho}{\partial s})_p s',\\
&\left(\frac{\partial\rho}{\partial p}\right)_s=\frac{\rho}{\gamma p}=\frac{\rho_0}{\gamma p_0}=\frac{1}{c^2},\\
&\left(\frac{\partial\rho}{\partial s}\right)_p=\left(\frac{T\partial\rho}{\partial q}\right)_p=\left(\frac{-\rho_0\partial T}{\partial q}\right)_p=-\frac{\rho_0}{C_p},
\end{aligned} \tag{14}$$

where c is the speed of sound, C_p is the heat capacity at constant pressure.

The entropy change is related to the heat fed into the medium as:

$$\mathrm{d}s=\mathrm{d}H/T,\quad H=\rho C_{\mathrm{V}}\frac{\partial T}{\partial t}, \tag{15}$$

where H is the heat transferred to the microelement.

The full-domain acoustic equation for the arc acoustic wave can be derived from the above equations:

$$\nabla^2 p'-\frac{1}{c^2}\frac{\partial^2 p'}{\partial t^2}=-\frac{\gamma-1}{c^2}\frac{\mathrm{d}H}{\partial t}, \tag{16}$$

where γ is the adiabatic coefficient, equal to C_p/C_{V}.

In the region outside the arc where there is no heat feedthrough H is 0, i.e., the common passive acoustic wave equation.

The sound pressure calculation domain is a sphere in diameter of 30 cm in 30 cm centred on the arc, as shown in Fig. 6. The initial sound pressure is relative to the ambient pressure and is set to 0. The outside boundary is defined as an acoustic impedance matching boundary with an acoustic impedance of 413 Pa·s/m, calculated using the formula

$$Z_{\mathrm{s}}=\rho_0 c_0, \tag{17}$$

where Z_{s} is the acoustic impedance, and ρ_0 and c_0 are the air density and speed of sound at 20 °C, with values of 1.2 kg/m^3 and 344 m/s, respectively.

Finally, it must be explained here that the fluid is compressible in the arc plasma model and incompressible in the acoustic model. The different descriptions are used because the spatial scales of the arc plasma model and the acoustic wave model are different. The arc model is concerned with spatial scales on the order of millimeters, while the acoustic wave model is concerned with spatial scales on the order of decimeters. Therefore, an approximation is taken in order to calculate far-field acoustic waves. The pressure perturbation caused by the arc after stabilization is not significant (as can be seen from the acoustic pressure) and the approximation can be considered reasonable.

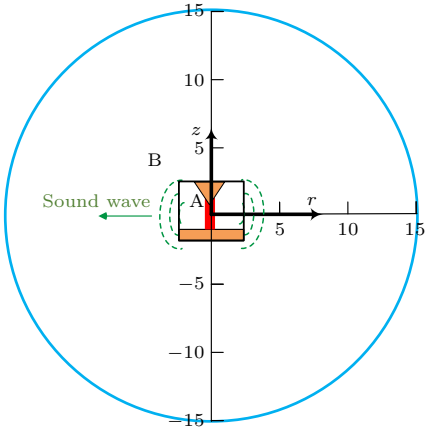


Fig. 6. Sound field calculation domain.

4. Results and discussion

In previous studies we have compared the model calculations with experimental results to show that the model is reliable.[1]

In order to investigate the effect of different gas media on the acoustic characteristics of the arc, the arc current and arc length were fixed in the experiment. The arc parameters are set as follows: arc current DC component I_{DC} is 100 A, AC component I_{AC} is 40 A, arc length L is 4 mm, and frequency f is 240 Hz.

4.1. Comparing arc acoustic waves

Figure 7 illustrates the sound pressure waveforms of arc sound measured at 15 cm from the center of the arc in argon, helium, and nitrogen. It can be observed that the morphology of the three arc sound pressure waveforms is basically the same. The waveform quality of the nitrogen arc sound pressure is poorer, which is caused by the fact that the arc combustion in nitrogen is not as stable as in argon and helium. In terms of sound pressure amplitude, argon arc sound pressure amplitude is the smallest, about 0.78 Pa. Nitrogen arc sound pressure amplitude is slightly higher than that of argon arc, about 0.83 Pa, for argon arc sound pressure 1.06 times. The helium arc has the highest sound pressure amplitude of about 1.41 Pa, which is about 1.81 times the sound pressure of the argon arc.

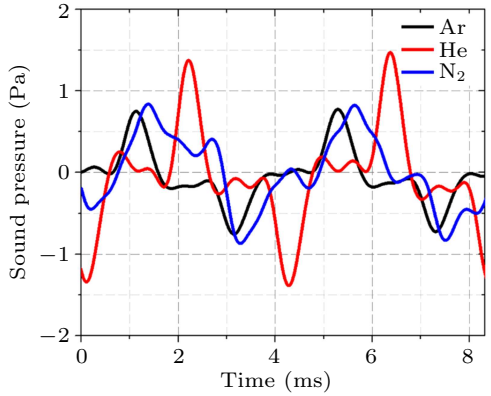


Fig. 7. Sound pressure waveforms of arc acoustic waves in three gases.

The physical process of the arc to generate sound waves can be divided into three stages:

Stage 1 Arc current to generate arc power.

Stage 2 Arc power heating arc.

Stage 3 The expansion and contraction of the arc to generate sound waves.

Therefore, the factors affecting the arc sound wave also correspond to the following three aspects.

(i) Arc voltage

It determines the amount of electric power that can be produced for the same arc current.

(ii) Electric–thermal efficiency

It determines the amount of thermal power that can be produced by the same electric power.

(iii) Thermal–acoustic efficiency

It determines the strength of the arc sound wave produced by the same thermal power.

From Eq. (16), the thermal–acoustic efficiency is always the same. Therefore, the intensity of the sound waves of different gas arcs depends on the voltage and electric–thermal efficiency. The higher the voltage, the higher the electric power, the larger the sound wave produced. The higher the thermal efficiency, the higher the internal energy power in the arc column, and the larger the sound wave generated. In addition, the electric–thermal efficiency is difficult to calculate because the physical quantity of arc thermal energy is not easy to measure. Therefore, the electric–acoustic efficiency, i.e., the ratio of the acoustic pressure to the AC component of the arc power, was measured directly in the experiment. Since the thermal-acoustic efficiency is always constant, the electric–acoustic efficiency is equivalent to the electric–thermal efficiency.

4.2. Comparing arc voltage

As the arc sounding characteristics are closely related to the electrical power deposited in the arc channel, the electrical characteristics of three gas arcs need to be discussed.

Figure 8 shows the voltage waveforms of the three gas arcs. It can be noted that for the same current waveform, the nitrogen arc has the highest voltage, the helium arc has the middle voltage and the argon arc has the lowest voltage. The

average voltages of the three arcs were calculated. The arc voltage drop (average value) for the argon arc is about 13 V or so. The arc voltage drop (average value) for the helium arc is about 19 V or so, which is about 1.5 times that of the argon arc. The arc voltage drop of the nitrogen arc is about 31 V or so, which is about 2.4 times that of the argon arc.

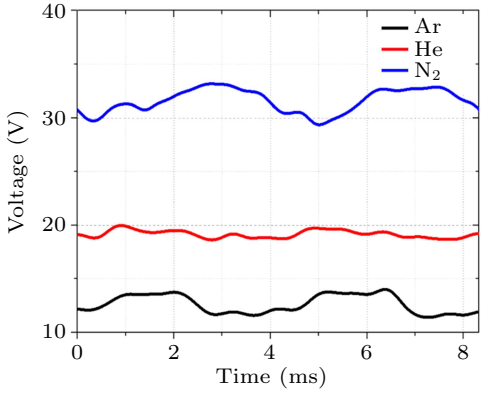


Fig. 8. Voltage waveforms of arcs in three gases.

To explain this phenomenon, numerical simulations of each of the three arcs were performed. Figure 9 shows the spatial distribution of the conductivity of the three arcs obtained by numerical simulation. It can be found that the maximum value of the conductivity of the three arcs does not differ much, but the argon arc has the widest distribution area of high conductivity and the nitrogen arc has the smallest distribution area of the highest conductivity. Equation (18) is the formula for the conductance, where G is the total conductance of the medium, σ is the specific conductance of the medium, S is the cross-sectional area, and l is the total length. From the formula, it can be known that the total conductance of the medium is directly proportional to the cross-sectional area. The argon arc has the widest distribution of high conductivity, i.e., the largest cross-sectional area, so the total conductance is the largest and the arc voltage drop is the lowest. Nitrogen arc is vice versa.

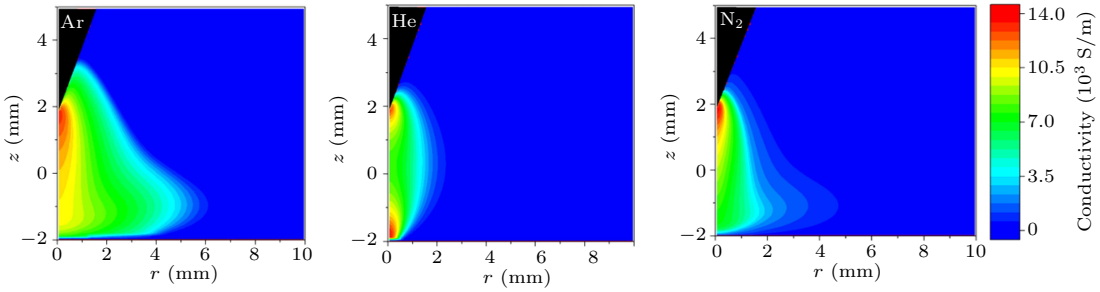


Fig. 9. Spatial distribution of conductivity of the arc in the three gases.

The reason for the different conductivity distributions of these three arcs can be explained by Fig. 10. As can be noted, the helium conductivity curve is much lower than that of argon, so the high conductivity region of the helium arc is smaller than that of the argon arc. Although the conductivity curve of nitrogen is close to that of argon, the high-temperature region of the nitrogen arc is smaller than that of the argon arc (as will be given in the temperature distribution below), so the high-conductivity region of the nitrogen arc is smaller than that of the argon arc.

$$G = \sigma S/l. \tag{18}$$

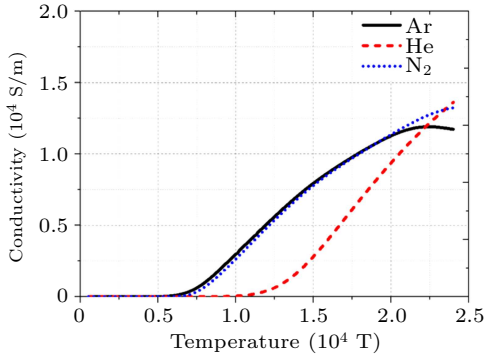


Fig. 10. Variation of conductivity with temperature for the three gases.

Figure 11 shows the temperature distribution of the arc under the three gases. It can be observed that the temperature distribution of the arc under the three gases is quite different. The temperature distribution of the argon arc presents a "bell-shaped", that is, near the cathode, the high temperature region is very narrow, while near the anode, the high temperature region is wider. And from the cathode to the anode, the temperature shows a decreasing trend. The temperature distribution of the helium arc is "pear-shaped", i.e., near the anode, the helium arc has a more obvious contraction, and the overall temperature of the helium arc is lower than that of the argon arc. And from the cathode to the anode, the temperature shows a trend of decreasing and then increasing. The temperature distribution of the nitrogen arc shows a "boot-shaped", similar in shape to the argon arc. However, near the cathode, its high temperature region is narrower than that of argon arc.

Figure 12 shows the morphology of the three gas arcs captured with the camera. It can be compared to see that the morphology of the experimentally captured arcs is roughly the same as the morphology of the arc temperature distribution obtained from the numerical simulation. The accuracy of the experiments and simulations are corroborated by each other.

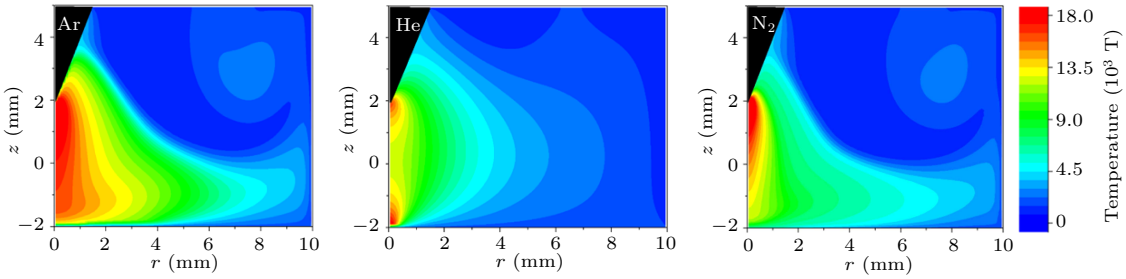


Fig. 11. The temperature distribution of the arc under the three gases.

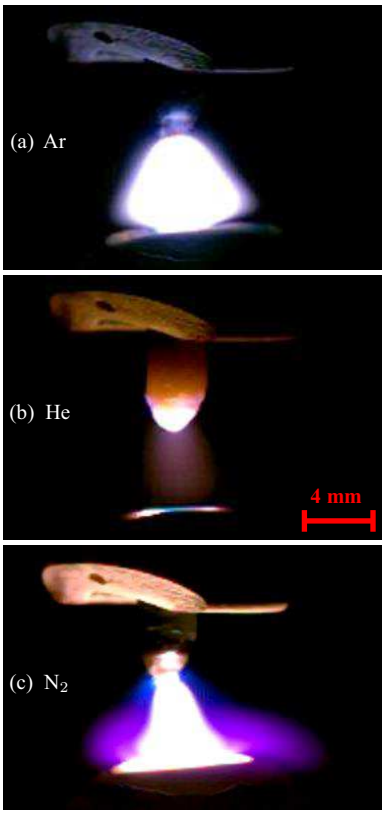


Fig. 12. The morphology of the arcs captured under the three gases.

The temperature distribution characteristics[28,29] of the arc are mainly determined by the thermal conductivity of the gas. The amount of heat transferred per unit area of gas by thermal conduction (also known as heat flow density) can be expressed as

$$\phi = -k'\nabla T, \tag{19}$$

where ϕ is the heat flow density, k' is the thermal conductivity, and T is the temperature.

When the thermal conductivity is large, the gas heat flow density is large and the gas dissipates heat very quickly. In order to ensure the balance between heat production and heat dissipation, the gas must reduce the heat dissipation power by reducing the heat dissipation area. For the arc with columnar distribution, the way to reduce the heat dissipation area is to reduce the radius of the arc channel. Its performance in the arc temperature distribution graph is the arc area is narrow.

The variation of thermal conductivity with temperature for the three gases is shown in Fig. 13. Since the thermal conductivity of helium is much larger than that of argon, the arc channel radius of helium is smaller than that of argon. In the temperature range above 10^4 K, the thermal conductivity of nitrogen is slightly larger than that of argon, which makes the nitrogen arc narrower than the argon arc in this temperature range. And in the interval of gas temperature of 0.5×10^4 K–1.0×10^4 K, nitrogen thermal conductivity is very large, making the nitrogen arc in this temperature interval is very narrow. But in the 5000 K below, the nitrogen thermal conductivity is reduced to very low, almost the same as argon, which makes the nitrogen arc in this temperature interval is wider. As can be seen in Fig. 11, the temperature distributions of argon and helium arcs are relatively similar in the region of $r > 6$ mm (where the temperature basically drops below 5000 K).

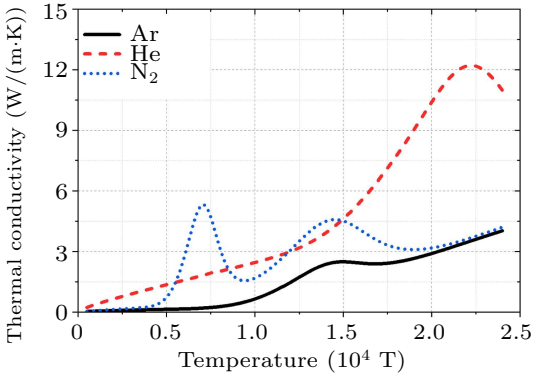


Fig. 13. The variation of thermal conductivity with temperature for the three gases.

4.3. Comparing electric–acoustic efficiency

Electric–acoustic efficiency is the intensity of sound waves that can be produced per unit change in electric power. Arc voltage and arc sound pressure have been measured experimentally above. Since the currents are the same, the electric–acoustic efficiency can be directly defined as the ratio of sound pressure to arc voltage. The electric–acoustic efficiencies of the argon, helium and nitrogen arcs were calculated to be approximately 0.052 Pa/V, 0.075 Pa/V, and 0.027 Pa/V, respectively. So, at the same arc current, helium arc has the highest electric–acoustic efficiency, argon arc is second and nitrogen arc is the lowest.

It has been pointed out above that electric–acoustic efficiency is equivalent to electric–thermal efficiency. Thus, we next discuss the differences in the electric–thermal efficiencies of the three arcs, i.e., the different internal energy powers produced by the same change in electric power. The arc electric power P is equal to the sum of the arc internal energy power H and the arc heat dissipation power Q. The internal energy power can be calculated by Eq. (15). Figure 14 illustrates the variation of the internal energy power and heat dissipation power of the three arcs during the variation of electric power, where the electric power is normalized (minimum value is 0 and maximum value is 1). It can be seen that for the same change in electric power, helium has the highest internal energy power, argon the next highest and nitrogen the lowest.

It can also be noted from Fig. 14 that for the same change in electric power, the magnitude of the internal energy power of the arc depends on how fast or slow the heat dissipation power responds to the change in electric power. The faster the response of the heat dissipation power, the smaller the internal energy power, and vice versa. Nitrogen arc has the fastest response of heat dissipation power and helium arc has the slowest. Thus, the nitrogen arc has the smallest internal energy power and the helium arc has the largest.

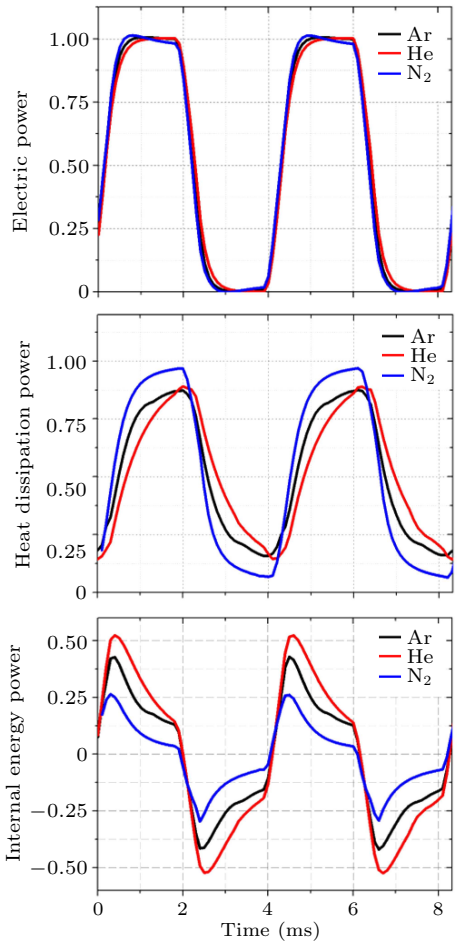


Fig. 14. Thermal processes inside the arc of the three gases.

The fundamental reason for this phenomenon is as follows: when the electric power is constant, the electric power and the heat dissipation power will reach an equilibrium state, in which the internal energy power is zero and the gas temperature remains constant. When the electric power changes, the heat dissipation power will change with the electric power, but relative to the electric power has a certain lag, and will eventually be consistent with the electric power, so as to achieve a new equilibrium state. During this change in equilibrium, internal energy power is generated, which is also responsible for the change in temperature. The magnitude of the internal energy power depends on how quickly the heat dissipation power responds to changes in electrical power. If the heat dissipation power response is especially fast (i.e., as soon as the injected electrical power is increased, it is immediately dissipated), the internal power generated in the arc channel is small, and vice versa.

Since the heat dissipation of the arc mainly depends on the heat dissipation of the anode, we will discuss the speed of the anode heat dissipation response in different gases. The speed of anode heat dissipation response is mainly influenced by two factors: (i) the heat dissipation area on the anode surface; (ii) the magnitude of thermal conductivity of the gas in the vicinity of the anode.

When the heat dissipation area on the anode surface is large, the heat dissipation is easy and the heat dissipation response is fast, and vice versa. The temperature gradient distribution of the three gas arcs is shown in Fig. 15. Since the temperature gradient represents the heat flow trend, the wider the range of high temperature gradient region on the anode surface, the larger the heat dissipation area and vice versa. As can be seen from the figure, the helium arc has a very narrow range of high temperature gradient region due to its obvious contraction near the anode, and therefore the heat dissipation area is very small. This leads to the difficulty of helium arc heat dissipation through the anode and the slow response of heat dissipation power. The argon arc and nitrogen arc have a wide range of high temperature gradient region, so the heat dissipation area is very large, the heat dissipation is easier, and the heat dissipation power response is fast.

Heat at a certain distance from the anode first needs to be transferred to the surface of the anode through the gas medium, and then dissipated through the anode, hence the gas thermal conductivity also has a large impact on heat dissipation. The distribution of the thermal conductivity of the three gas arcs is shown in Fig. 16. As can be seen from the figure, the thermal conductivity of the argon arc is the lowest overall, followed by the helium arc, but the higher thermal conductivity region of the helium arc is mainly concentrated near the axis of the arc (the area of helium arc with thermal conductivity higher than 2 W/(m·K) is even smaller than that of argon arc). The thermal conductivity distribution region of the nitrogen arc is much larger than that of the argon and helium arcs, which results in a fast power response of the nitrogen arc to dissipate heat.

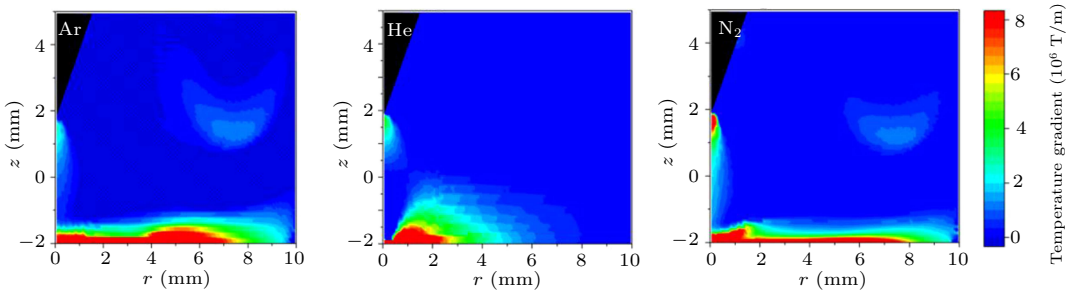


Fig. 15. Temperature gradient distribution of the three gas arcs.

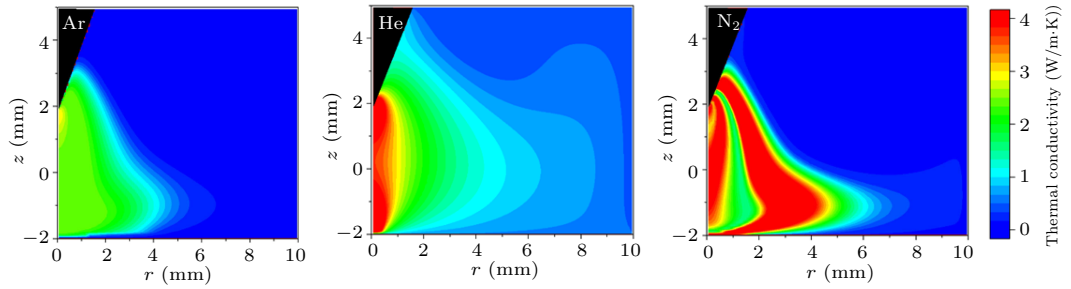


Fig. 16. The thermal conductivity distribution of the three gas arcs.

Combining the two factors discussed above, the nitrogen arc has the fastest heat dissipation response (both high thermal conductivity and large heat dissipation area), the argon arc is second (low thermal conductivity but large heat dissipation area), and the helium arc is the slowest (too small heat dissipation area). Therefore, in the same electric power change process, helium arc internal energy power is the largest, argon arc is the second, nitrogen arc is the smallest. This results in the helium arc producing the strongest sound waves, the argon arc the next strongest, and the nitrogen arc the smallest.

5. Conclusion

In this paper, DC bias alternating arc sound waves in three gases (argon, helium, and nitrogen) are investigated experimentally and by simulation. It is found that there are large differences in the arc sound waves of different gases. The reasons for the differences mainly depend on two factors: the voltage drop of the arc and the electric–acoustic conversion efficiency. The voltage drop of the arc determines the magnitude of the electrical power within the arc channel. The electric–acoustic conversion efficiency determines the amount of internal energy power in the arc channel. Under the same driving current, the voltage drop is nitrogen arc, helium arc, argon arc in descending order, and the electric–acoustic conversion efficiency is helium arc, argon arc, nitrogen arc in descending order. This research deepens the understanding of the physical processes involved in arc acoustic waves and contributes to the selection of gas environments for arc acoustic applications.

Acknowledgement

Project supported by the National Natural Science Foundation of China (Grant Nos. 51877118 and 52077117).

References

[1] Chen Z, *et al*. 2019 *IEEE Trans. Plasma Sci.* **47** 4136
[2] Aleksandar Jovic 2014 Ph. D. thesis (Sweden: Luleå University of Technology)
[3] Klein S 1954 *Acustica* **4** 77
[4] Yvonne S, *et al*. 2011 *IEEE Trans. Plasma Sci.* **39** 2146
[5] Naidis G V 2012 *Plasma Sources Sci. Technol.* **21** 025009
[6] Eugene A 1961 *J. Acoust. Soc. Am.* **33** 1708
[7] Li H, *et al*. 2021 *Phys. Plasmas* **28** 073502
[8] Severinsen D and Gupta G S 2013 *Proceedings of the World Congress on Engineering* 2013
[9] Sagar S, *et al*. 2014 *International Journal of Scientific & Engineering Research* **5** 572
[10] Fitaire M and Mantei T D 1972 *Phys. Fluids* **15** 464
[11] Sforzini M, *et al*. 1975 *IEEE Transactions on Power Apparatus and System* **94** 591
[12] Li Y, *et al*. 2021 *Phys. Plasmas* **28** 073510
[13] Cunha MD, *et al*. 2023 *J. Phys. D: Appl. Phys.* **56** 395204
[14] Li Y, *et al*. 2022 *Plasma Sources Science & Technology* **31** 045027
[15] Liu Z, *et al*. 2023 *J. Appl. Phys.* **134** 233301
[16] Kuwahara T and Asaka Y 2024 *J. Magn. Magn. Mater.* **589** 171572
[17] Xue W, Kusumoto K and Nezu K 2003 *Science and Technology of Welding and Joining* **8** 443
[18] Roca A S, *et al*. 2009 *Science and Technology of Welding and Joining* **14** 117
[19] Macias E J, *et al*. 2010 *Science and Technology of Welding and Joining* **15** 26
[20] Pal K and Pal S K 2011 *Materials and Manufacturing Processes* **26** 684
[21] Strekalov M L 2024 *Chem. Phys. Impact* **8** 100444
[22] Michael S M and Marshall M 1987 *J. Acous. Soc. Am.* **81** 1972
[23] Chen Z, *et al*. 2020 *Phys. Plasma* **27** 023509
[24] Hsu K C, Etemadi K and Pfender E 1983 *J. Appl. Phys.* **54** 1293
[25] Raizer Y P 1991 *Gas Discharge Physics* (Berlin: Springer-Verlag)
[26] Hsu K C 1982 Ph. D. thesis (University of Minnesota)
[27] Evans D L and Tankin R S 1967 *Phys. Fluids* **10** 1137
[28] Zheng B, *et al*. 2023 *Chin. Phys. B* **32** 095203
[29] Chen J, *et al*. 2022 *Chin. Phys. B* **31** 065205